Vietnam Journal of Catalysis and Adsorption
Tạp chí xúc tác và hấp phụ Việt Nam

http://jca.edu.vn

# Novel synthesis of CoS/C composite as an anode material for Li-ion batteries

Nguyen Phi Hung[1], Pham Trung Kien[2], La Duc Duong[2], Phan Thi Thuy Trang[1], Nguyen Thi Lan[1], Nguyen Van Kim[1], Vo Vien[1,*]

[1] *Faculty of Natural Sciences, Quy Nhon University, 170 An Duong Vuong, Quy Nhon Nam, Gia Lai*
[2] *Institute of Materials, Biology and Environment, 17 Hoang Sam, Nghia Do, Hanoi*
** Email: vovien@qnu.edu.vn*

ARTICLE INFO

Received: 04/06/2026
Accepted: 29/06/2026
Published: 30/06/2026

*Keywords:*
cobalt sulfide/carbon;
cobalt disulfide/graphitic;
carbon nitride;
lithium-ion battery

ABSTRACT

In this study, cobalt sulfide/carbon nanocomposites were successfully synthesized via a temperature-controlled pyrolysis method using cobalt salt and thiourea as precursors. The results demonstrate that the calcination temperature plays a key role in governing the phase structure and lithium-storage performance of the resulting materials. At a calcination temperature of 550 °C (sample CS-550), a cubic $CoS_2$ phase coexists with partially decomposed g-$C_3N_4$. Meanwhile, at 630 °C (sample CS-630), the material completely transforms into a highly crystalline hexagonal CoS phase encapsulated by a highly conductive graphitized carbon shell. The CS-630 electrode exhibits superiority over CS-550 in terms of both electrochemical kinetics and mechanical durability during the lithiation/delithiation processes. Specifically, CS-630 delivers a stable discharge capacity of approximately 358.51 mAh $g^{-1}$ after 200 cycles, which is higher than that of CS-550 (only ~69.64 mAh $g^{-1}$ after 180 cycles). Furthermore, the CS-630 anode possesses lower charge-transfer resistance, enhanced $Li^+$ ion diffusion capabilities compared to CS-550. This superior performance is credited to the robust hexagonal CoS framework synergized with the conductive carbon network, which effectively accelerates electrochemical kinetics and buffers the volumetric strain induced during cycling. This work underscores that tailoring the calcination temperature is an effective strategy for enhancing the performance of cobalt sulfide anodes in lithium-ion batteries.

## Introduction

In recent years, the growing demand for advanced portable electronics and electric vehicles (EVs) has stimulated extensive research into next-generation anode materials for lithium-ion batteries (LIBs) to replace commercial graphite [1]. Among the candidate materials, cobalt sulfide-based ($CoS_x$) systems have garnered substantial interest due to their high practical capacities and favorable electrochemical reaction kinetics [2]. Among various cobalt sulfides, a large portion of existing literature has dedicated attention to the cobalt disulfide ($CoS_2$) phase with the theoretical specific capacity of 872 mAh $g^{-1}$. Furthermore, $CoS_2$ can be readily synthesized with high phase stability under moderate hydrothermal conditions (160 – 200 °C) [3]. Nevertheless, $CoS_2$-based anodes routinely face challenges regarding long-term cycling stability. The simultaneous accommodation of multiple $Li^+$ ions within the rigid cubic lattice typically induces large volume



https://doi.org/10.62239/jca.2026.032

fluctuations, easily leading to the mechanical pulverization of active particles and subsequent rapid capacity fading upon extended operation. To mitigate this issue, a widely adopted strategy involves combining $CoS_2$ with various supporting matrices, most commonly carbonaceous materials [1-3].

To optimize the charge-transport kinetics and enhance the mechanical durability of this material system, this study proposes a tailored approach by adjusting the pyrolysis temperature to 630 °C to drive phase transformation and refine the carbon matrix quality. Although the hexagonal CoS phase delivers a lower theoretical capacity (589 mAh $g^{-1}$), its highly symmetric hexagonal crystal configuration is known for its structural robustness and superior tolerance against volumetric strain [4]. Results in this work indicate that the sample optimized at 630 °C exhibits noticeably improved electrochemical performance and structural stability compared to at 550 °C. We demonstrate that elevating the temperature to 630 °C provides an appropriate thermodynamic driving force for desulfurization, leading to a complete transition into the stable hexagonal CoS phase, while effectively eliminating the poorly conductive organic functional groups of g-$C_3N_4$. The concomitant gas evolution generates an interconnected porous nanostructure that serves as a physical buffer to accommodate volume variations. This study contributes a balanced experimental perspective on reconciling the trade-off between theoretical capacity and mechanical lifespan via precise inorganic phase engineering and carbon matrix refinement for energy storage applications. For the first time to the best of our knowledge, we focus on the synthesis of $CoS_x$ materials at different calcination temperatures to investigate the effects of temperature on phase formation, structural characteristics, and electrochemical performance. The findings of this study are expected to provide valuable guidelines for the development of high-performance cobalt sulfide electrode materials for lithium-ion battery applications.

## Experimental section

### *Chemicals and Reagents*

All chemicals used in this study were purchased from Sigma-Aldrich (Germany) and used as received without further purification. These reagents included: thiourea ($(NH_2)_2CS$, 99.0%), cobalt(II) acetate tetrahydrate ($(CH_3COO)_2Co.4H_2O$, 99.0%), anhydrous ethanol ($C_2H_5OH$, 99.5%), polyvinylidene fluoride (PVDF, 99.0%), and N-methyl-2-pyrrolidone (NMP, 99.0%). For cell fabrication, copper (Cu) foil, lithium (Li) metal foil (99.9%), lithium hexafluorophosphate ($LiPF_6$, 99.99%), ethylene carbonate (EC, 99%), and dimethyl carbonate (DMC, 99%) were utilized.

### *Material synthesis*

In a typical procedure, a solid mixture of $(NH_2)_2CS$ and $Co(CH_3COO)_2.4H_2O$ was thoroughly blended at a 1:1 mass ratio. The mixture was then transferred into a tube furnace and calcined under a continuous Argon (Ar) atmosphere. To investigate the temperature effects, the thermal treatment was executed at two distinct targeted temperatures: at 550 °C for 4 h (denoted as CS-550) and at 630 °C for 4 h (denoted as CS-630). For both samples, a constant heating rate of 10 °C $min^{-1}$ was maintained. The as-calcined products were collected and washed twice with distilled water, followed by a final washing step with anhydrous ethanol. Finally, the obtained powders were dried in a vacuum oven at 80 °C for 12 h.

### *Characterization of materials*

The phase compositions of the samples were investigated by X-ray diffraction (XRD) using a Bruker D2 diffractometer with Cu-Kα radiation (λ = 1.5406 Å), operating at voltage of 30 kV and current of 10 mA (0.01 A). Fourier-transform infrared (FT-IR) spectra were recorded on a PerkinElmer Spectrum GX spectrometer. The morphologies were examined via scanning electron microscopy (SEM) on a Nova NanoSEM 450 system, while elemental compositions were determined by energy-dispersive X-ray spectroscopy (EDS) equipped on a JEOL JSM-5410 framework. Raman scattering spectroscopy was performed on a Horiba XploRA Plus micro-Raman spectrometer to evaluate the carbon structural disorder and graphitization degree.

### *Electrochemical characterization*

The working electrodes were fabricated by blending the active material (70 wt%), conductive carbon black (15 wt%), and polyvinylidene fluoride (PVDF) binder (15 wt%) in N-methyl-2-pyrrolidone (NMP) solvent to form a homogeneous slurry. The resultant slurry was then uniformly coated onto copper foil current collectors (diameter: 1.2 cm, corresponding to a radius r = 0.6 cm) and subsequently dried in a vacuum oven at 70 °C for 24 h. CR2032 coin-type cells were assembled inside an Argon-filled glove box. Lithium metal foil was employed as the counter and reference electrode. The electrolyte consisted of a 1.0 M $LiPF_6$ solution dissolved in a mixture of ethylene carbonate (EC) and dimethyl carbonate (DMC) at a 1:1 volumetric ratio, with approximately 50 µL introduced into each cell. A porous polyethylene membrane was utilized as the separator.

https://doi.org/10.62239/jca.2026.032

The electrochemical performance was evaluated by galvanostatic charge/discharge measurements within a voltage window of 0.1–3.0 V (vs. $Li/Li^+$). The cells were cycled at a specific current density of 100 mA $g^{-1}$ for the first five initial cycles to stabilize the electrode, and subsequently tested at a higher current density of 1000 mA $g^{-1}$ for the remaining extended cycles.

## Results and discussion

### *Characterization of materials*

As shown in Figure 1a, the XRD pattern of CS-550 exhibits well-defined diffraction peaks at 2 theta of 27.89°, 32.32°, 36.26°, 39.86°, 46.36°, and 54.97°, which are indexed to the (111), (200), (210), (211), (220), and (311) planes, respectively, which corresponds to the cubic cobalt disulfide ($CoS_2$) crystal structure belonging to the Pa-3 space group [3].

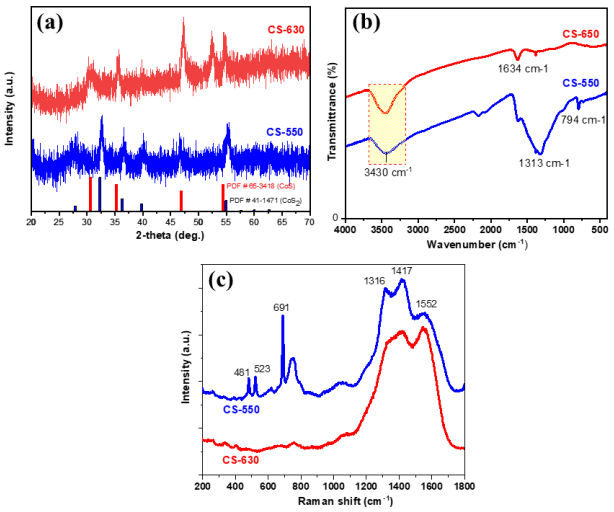


Figure 1. XRD patterns (a), IR (b) and Raman (c) spectra of CS-550 and CS-630 ~~materials~~.

For CS-630, the characteristic diffraction peaks of the $CoS_2$ phase completely vanish. Instead, the pattern reveals sharp and high-intensity reflections at 2 theta values of 30.5°, 35.3°, 47.0°, and 54.3°, which are assigned to the (100), (101), (102), and (110) planes of the hexagonal cobalt sulfide (CoS) phase [4]. Furthermore, CS-630 exhibits noticeably sharper and narrower diffraction peaks, indicating a higher degree of crystallinity compared to CS-550, which may be beneficial for boosting the electronic conductivity and strengthening the structural integrity of the electrode during continuous lithiation/delithiation processes.

Figure 1b reveals a distinct evolution in the chemical bonding of surface functional groups as the calcination temperature increases from 550 °C to 630 °C. For CS-550, the spectrum displays a broad absorption band centered at approximately 3430 $cm^{-1}$, which is characteristic of the stretching vibration of –OH groups from physically adsorbed surface moisture [5]. Additionally, several intense peaks emerging within the 1390–1634 $cm^{-1}$ region are assigned to the characteristic stretching vibrations of heterocyclic C–N and C=N bonds [6]. This observation confirms that at 550 °C, the thermal decomposition of the organic components remains incomplete, resulting in a composite material characterized by a cubic $CoS_2$ phase integrated with a carbon nitride matrix derived from the partial pyrolysis of thiourea. Besides, a weak peak at 619 $cm^{-1}$ can be attributed to Co-S bond [6]. For CS-630, the absorption peak at 1634 $cm^{-1}$ almost completely vanishes, indicating the thorough decomposition of the C=N/C–N heteroring structures. Furthermore, the intensity of the –OH stretching band at 3430 $cm^{-1}$ drops drastically compared to that of CS-550, demonstrating a significantly minimized amount of adsorbed water and residual surface functional groups after the high-temperature treatment. The formation of a well-crystallized hexagonal CoS phase with reduced organic impurities is highly anticipated to enhance electronic conductivity and facilitate $Li^+$ ion transport pathways when employed as an anode material for lithium-ion batteries. Remarkably, a weak peak around 610 $cm^{-1}$ can be assigned to Co-S bond [6].

The Raman spectra are illustrated in Figure 1c. For CS-550, several scattering peaks located between 794 and around 1313 $cm^{-1}$ are assigned to the characteristic stretching vibrations of aromatic rings within the g-$C_3N_4$ network [7, 8]. Additionally, the Raman peaks emerging at 1552 $cm^{-1}$ and 1316 $cm^{-1}$ correspond to the well-known G-band and D-band of carbonaceous materials, respectively. Specifically, the G-band is associated with the $E_{2g}$ stretching vibration mode of $sp^2$-hybridized carbon atoms within the graphitic lattice, whereas the D-band is closely related to the structural defects, disordered carbon, and edge distortions [9]. These features confirm that at a moderate calcination temperature of 550 °C, the material exists as a $CoS_2$/g-$C_3N_4$ composite, which is in highly consistent agreement with the FT-IR results. For CS-630, the characteristic Raman peaks of g-$C_3N_4$ almost entirely fade away. Concurrently, the disappearance of these g-$C_3N_4$ signals implies a transition from the $CoS_2$/g-$C_3N_4$ composite system to a well-defined CoS/C system. Consequently, the pristine carbon-encapsulated hexagonal CoS framework in CS-630 is highly expected to deliver superior electronic conductivity and faster $Li^+$ ion transport kinetics when employed as an anode material for lithium-ion batteries.

https://doi.org/10.62239/jca.2026.032

The morphologies and elemental compositions of CS-550 and CS-630 were investigated via SEM and EDS (Figure 2). Figure 2a reveals large sheets, which is attributed to the incomplete thermal decomposition of the organic precursors and the g-$C_3N_4$ skeleton at 550°C. CS-630 exhibits a more highly dispersed morphology composed of distinct, sharp-edged nanosheets with a relatively uniform size distribution (Figure 2b). The well-dispersed and porous architecture of CS-630 is highly beneficial for expanding the electrochemically active surface area with the electrolyte, shortening the diffusion pathways for $Li^+$ ions, and effectively buffering the localized volumetric strain during continuous lithiation/delithiation processes.

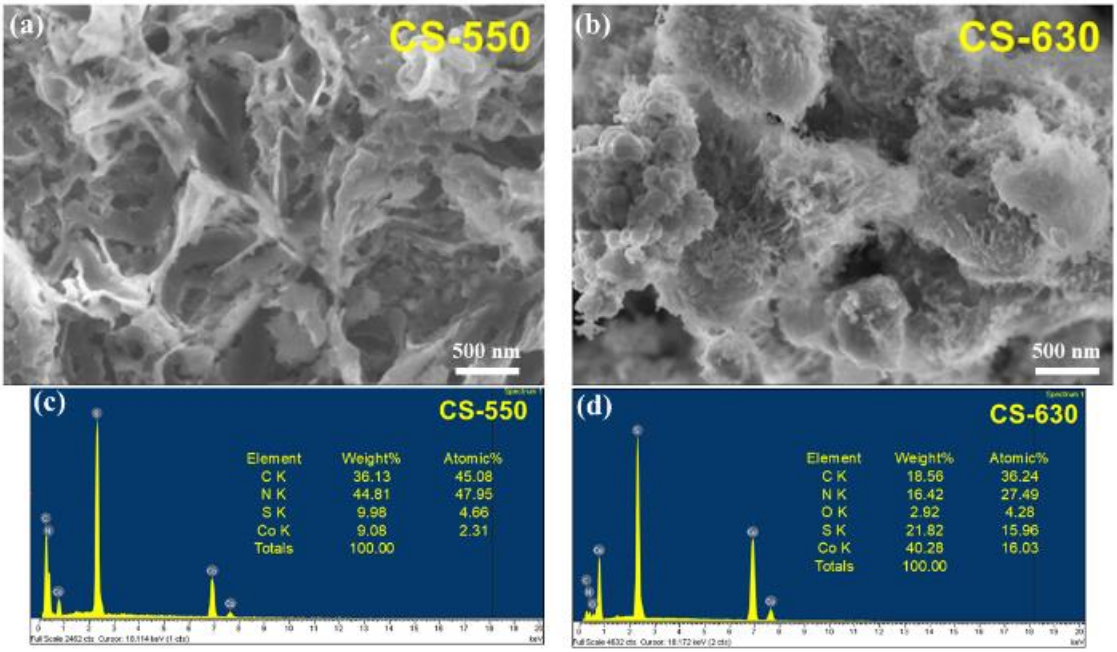


Figure 2. SEM images and EDS spectra of CS-550 and CS-630

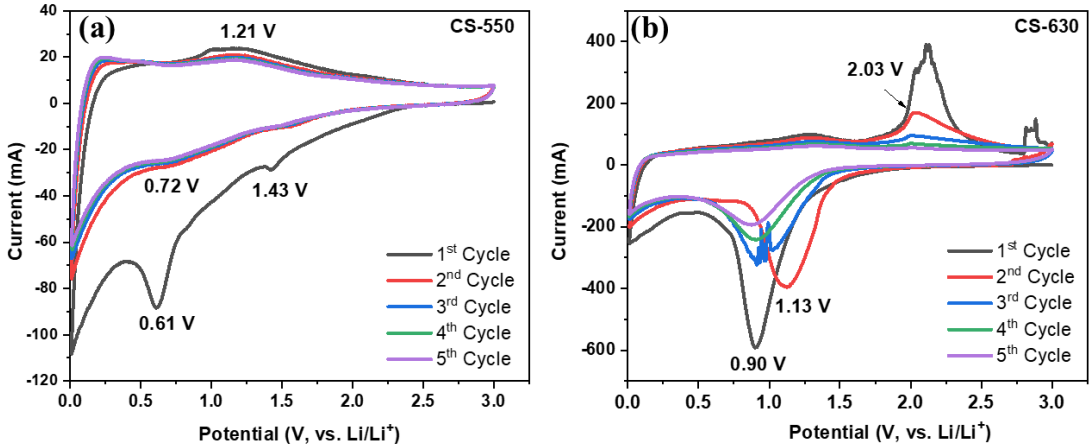


Figure 3. CV curves of CS-550 and CS-630.

The EDS spectrum (Figure 2c) shows the atomic ratio of Co to S is approximately 1:2, which is in consistent agreement with the cubic $CoS_2$ phase; and a relatively high content of nitrogen (N), verifying the structural residence of partially decomposed g-$C_3N_4$. For CS-630, the Co:S atomic ratio shifts close to 1:1, confirming the successful transition into the CoS phase. Concurrently, the N signal drops drastically, demonstrating that the insulating carbon nitride framework was almost completely eradicated at 630 °C. A sustained carbon signal is registered in both samples, indicating the robust establishment of a carbonaceous matrix encapsulating the inorganic materials.

https://doi.org/10.62239/jca.2026.032

*Electrochemical characterizaion*

The cyclic voltammetry (CV) of the samples is illustrated in Figure 3. For CS-550, the first cathodic scan exhibits peaks at 1.43 and 0.61 V. The first one is attributed to the multi-step intercalation of $Li^+$ ions into the $CoS_2$ lattice and the subsequent conversion reactions, following the equations [10]:

$$CoS_2 + x\ Li^+ + xe^- \rightarrow Li_xCoS_2 \quad (1)$$

$$Li_xCoS_2 + (4\text{-}x)\ Li^+ + (4\text{-}x)\ e^- \rightarrow Co + 2Li_2S \quad (2)$$

The second peak at 0.61 V may be typically accompanied by the decomposition of the electrolyte to form the solid electrolyte interphase (SEI) [10]. From the second cycle onward, the CV curves display near-perfect overlapping, indicating high electrochemical reversibility and stable lithiation/delithiation kinetics. The reduction peak at 0.72 V and the oxidation peak at 1.21 V are considered as the two peaks reflecting the reversible conversion process of the electrode [10].

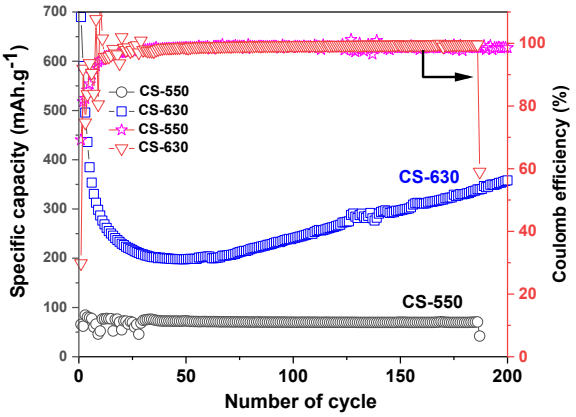


Figure 4. Specific capacity and Coulombic efficiency of the CS-550 and CS-630 electrodes.

For the CS-630 electrode, during the initial cathodic scan, a distinct reduction peak observed at approximately ~0.90 V is assigned to the SEI layer formation. This peak completely disappears in the subsequent cycles, confirming that a stable and robust SEI film has been successfully established. Concurrently, in the following two cycles, the main reduction peak shifts to a higher potential region (~1.13 V), reflecting an electrochemical activation process of the active material and a substantial improvement in reaction kinetics after the initial cycle. On the other hand, the prominent oxidation peaks recorded at approximately 2.03 V are attributed to the reversible anodic oxidation process, during which metallic Co is converted back into $Li_xCoS$ and hexagonal CoS phases. The good overlapping of the second and third CV curves underscores the excellent electrochemical reversibility and structural integrity of the optimized CS-630 electrode during continuous lithiation/delithiation processes. The reduction peak at around 1.00 V and the oxidation peak at 2.03 V are considered as the two peaks reflecting the reversible conversion process of the electrode [10].

The galvanostatic charge/discharge performance of the CS-550 and CS-630 electrodes is presented in Figure 4. CS-550 delivers a low capacity, about 65.66 mAh $g^{-1}$ for the first cycle and obtains 69.64 mAh $g^{-1}$ after 180 cycles, accompanied by a Coulombic efficiency of 99.57%. For the CS-630 electrode, it demonstrates remarkably enhanced capacity with a capacity of 689.64 mAh $g^{-1}$ and Coulombic efficiency of 69.16% for the first cycle. However, it decreases to ~ 200 mAh $g^{-1}$ after 50 cycles and then increases to 358.51 mAh $g^{-1}$ with an impressive Coulombic efficiency of 98.6% after 200 cycles. For the CS-630 electrode, in the first 50 cycles, the capacity may be degraded due to volume changes during cycling, causing electrode fragmentation, leading to some regions of active material being isolated from the electrolyte or the SEI layer becoming unstable. This is a common phenomenon in LIB anodes. However, in subsequent cycles, the liquid electrolyte begins to permeate deeper into the isolated parts deep within the particle core, activating previously unreacted material regions. Consequently, the contact surface between the Co nanoparticles and the electrolyte increases dramatically. At low potential, the organic electrolyte decomposes and forms a polymer/gel film around the particles. This film is capable of storing $Li^+$ ions through a reversible pseudo-capacitive "attachment-release" mechanism on the surface [11-13]. This result may be benefiting from the synergistic combination of the robust CoS framework and the highly conductive carbon network.

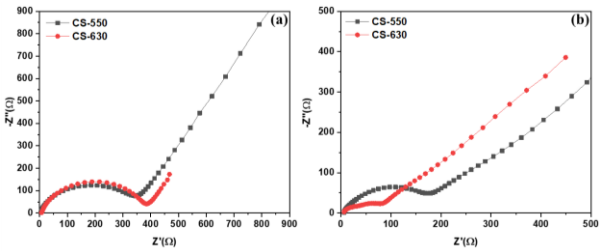


Figure 5. EIS spectra of the CS-550 and CS-630 electrodes at the pristine state (a) and the 50$^{th}$ cycle (b).

The electrochemical impedance spectroscopy (EIS) of the CS-550 and CS-630 cells were conducted at the pristine state and the 50$^{th}$ cycle (Figure 5). In their pristine state, both electrodes display semicircles with similar diameter in the high-to-medium frequency

https://doi.org/10.62239/jca.2026.032

region. However, after 50 cycles, CS-550 exhibits a larger semicircle diameter than CS-630, indicating a higher charge-transfer barrier. This difference is predominantly driven by the structural residence of the insulating g-$C_3N_4$ residues in CS-550, whereas the CS-630 framework incorporates a highly conductive graphitized carbon layer that significantly accelerates electronic transport pathways [14, 15].

To evaluate the morphological evolution and structural stability of the electrode materials after extended electrochemical operation, SEM examination of the cells was conducted after the 10$^{th}$ cycle (Figure 6).

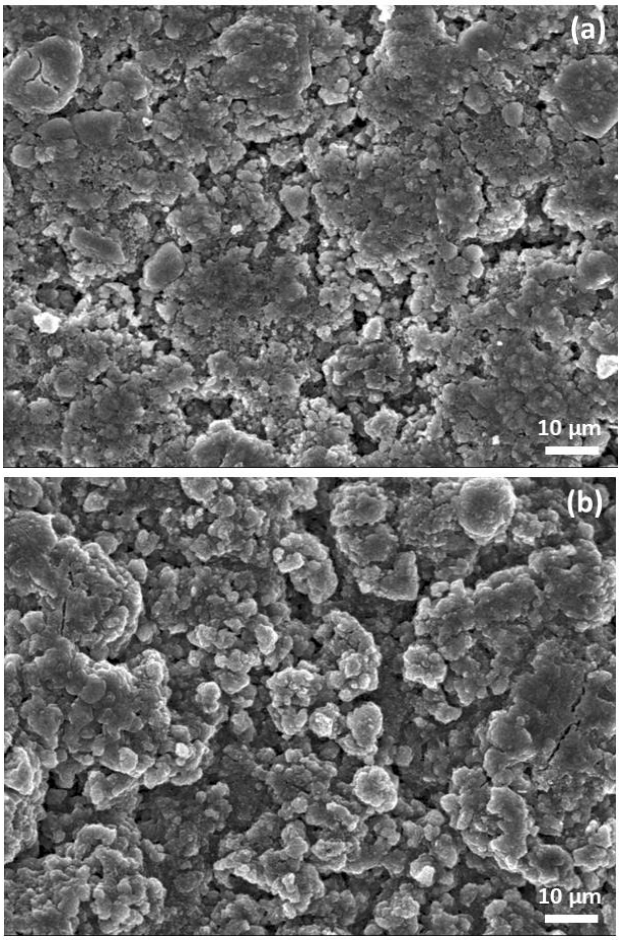


Figure 6. SEM images of the CS-550 (a) and CS-630 (b) anode after 10 cycles.

The post-cycling SEM micrographs of the CS-550 and CS-630 electrodes display a striking contrast in their structural endurance under electrochemical stress. For the CS-550 electrode, the electrode surface exhibits severe degradation, characterized by the propagation of numerous large, deep cracks after 10 cycles. This pulverization phenomenon demonstrates that the cubic $CoS_2$ framework possesses poor tolerance against volumetric expansion during continuous cycling, leading to irreversible mechanical failure and a catastrophic loss of electrical contact among the active nanoparticles. Furthermore, the structural residence of the insulating g-$C_3N_4$ residues restricts electronic transport, thereby exacerbating both structural degradation and capacity fading.

However, the optimized CS-630 electrode remarkably preserves its initial well-dispersed particulate morphology, with almost no visible structural fractures or severe cracking after 10 intensive cycles. This outstanding structural integrity proves that the hexagonal CoS phase, combined with the graphitized carbon shell generated at the higher calcination temperature, successfully functions as an integrated conductive network and a highly effective mechanical buffering matrix. This graphitized carbon coating not only accelerates electron transfer kinetics but also dynamically absorbs the localized internal stress induced by volume fluctuations during continuous lithiation/delithiation processes, thereby suppressing particle severe agglomeration and protecting the active material from pulverization. These post-cycling SEM observations are in seamless alignment with the aforementioned EIS data and long-term cycling profiles, thoroughly confirming the superior electrochemical stability and structural robustness of the CS-630 electrode over CS-550.

## Conclusions

In summary, cobalt sulfide/carbon nanocomposites were successfully synthesized via a temperature-controlled pyrolysis strategy, and the critical influence of the calcination temperature on the resulting phase configurations and lithium-storage performance was systematically elucidated. Structural analyses revealed that at a moderate temperature of 550 °C (CS-550), a cubic $CoS_2$ phase coexists with partially decomposed g-$C_3N_4$ residues. Conversely, elevating the temperature to 630 °C (CS-630) drives the exhaustive pyrolysis of the carbon nitride framework, yielding a phase-pure hexagonal CoS structure well-dispersed within a highly conductive graphitized carbon matrix. The optimized CS-630 anode exhibits overwhelming electrochemical superiority over CS-550. Specifically, CS-630 sustains a stable discharge capacity of approximately 358.51 mAh $g^{-1}$ after 200 extended cycles, which is substantially higher than that of CS-550 (only ~69.64 mAh $g^{-1}$). Post-cycling SEM observations further verified that the interconnected CoS/C architecture of CS-630 remarkably preserves its morphological integrity, effectively suppressing particle pulverization and severe agglomeration compared to the fragile $CoS_2$ framework

https://doi.org/10.62239/jca.2026.032

in CS-550. This work not only introduces a straightforward yet effective strategy to optimize the performance of transition metal sulfide anodes via precise temperature-driven phase engineering but also provides profound fundamental insights into tailoring phase structures and conductive carbon host networks for next-generation energy storage applications.

## Acknowledgments

This research is funded by Vietnam National Foundation for Science and Technology Development (NAFOSTED) under grant number 104.05-2021.84.

## References

1. H.R. Lee, S.Y. Lee, U.H. Son, S. Lee, H.-I. Joh, Appl. Surf. Sci., 664 (2024) 160228. https://doi.org/10.1016/j.apsusc.2024.160228
2. Z. Wang, L. Han, Y. Wang, Q. Liu, Z. Kong, X. Gao, J. Ye, Q. Liu, Y. Chen, G. Xia, Mater. Lett., 364 (2024) 136332. https://doi.org/10.1016/j.matlet.2024.136332
3. E. Chae, S. Myeong, M. Kang, B.K. Kim, T.-S. Bae, Y.-S. Lee, Carbon Lett., 36 (2026) 1049-1060. https://doi.org/10.1007/s42823-026-01053-2
4. Y. Liu, J. Energy Storage, 104 (2024) 114641. https://doi.org/10.1016/j.est.2024.114641
5. Y. Song, J. Yi, H. Chen, X. She, Z. Chen, C. Ding, H. Li, H. Xu, Appl. Surf. Sci., 467 (2019) 56-64. https://doi.org/10.1016/j.apsusc.2018.10.118
6. M.M. Danish, Ceram. Int., 47 (2021) 13043-13056. https://doi.org/10.1016/j.ceramint.2021.01.168
7. H. Li, X. Ma, T. Liu, L. Yang, B. Liu, S. Yin, Y. Wei, Y. Wang, RSC Adv., 7 (2017) 8688. https://doi.org/10.1039/c6ra26498k
8. P.V. Zinin, S.K. Sharma, V.N. Khabashesku, X. Liu, S. Hong, S. Endo, T. Acosta, Chem. Phys. Lett., 472 (2009) 69-73. https://doi.org/10.1016/j.cplett.2009.02.068
9. Á. Pérez-Molina, S. Morales-Torres, F.J. Maldonado-Hódar, Catal. Today, 418 (2023) 114608. https://doi.org/10.1016/j.cattod.2023.114068
10. S.-Y. Liao, S.-Y. Zhang, J.-J. Cai, F. Zheng, Y.-D. Liu, Y.-G. Min, Electrochim. Acta, (2019) 134992. https://doi.org/10.1016/j.electacta.2019.134992
11. H.T. Huu, T.N. Ngoc, N.S.M. Viswanath, M.T. Nguyen, T.H.T. Kim, V. Vo, M.V. Tran, H.N. Phi, J. Power Sources, 653 (2025) 237719. https://doi.org/10.1016/j.jpowsour.2025.237719
12. H.T. Huu, H.T.T. Le, V.P. Nguyen, T.T.H. Nguyen, T.X.D. Nguyen, V.T. Nguyen, S.-J. Kim, V. Vo, Electrochim. Acta, 341 (2020) 136010. https://doi.org/10.1016/j.electacta.2020.136010
13. H.T. Huu, H.T.T. Le, T.H. Nguyen, L.N. Thi, V. Vo, W.B. Im, Appl. Surf. Sci., 549 (2021) 149312. https://doi.org/10.1016/j.apsusc.2021.149312
14. X. Xiao, D. Wang, H. Wang, D.Y.W. Yu, A.L. Rogach, ACS Appl. Mater. Interfaces, 12 (2020) 12809-12820. https://doi.org/10.1021/acsami.9b22169
15. L. Guo, J. Wang, J. Liang, L. Xi, Electrochim. Acta, 322 (2019) 134763. https://doi.org/10.1016/j.electacta.2019.134763